Surface Science 266 (1992) 185–190
North-Holland

surface science

Microdroplet emission and instabilities in liquid-metal ion sources

V.V. Vladimirov, V.E. Badan and V.N. Gorshkov
Physics Institute, Ukrainian Academy of Sciences, Prospekt Nauki 46, 252650 Kiev GSP, Ukraine

Received 5 August 1991; accepted for publication 2 September 1991

When the liquid metal ion sources (LMIS) operate in the high-current mode, an instability arises which is accompanied by the comparatively low-frequency ion current oscillations and microdroplet emission. Two distinct groups of microdroplets are observed, the large ones (with radius higher than 10^3 Å) and the smaller ones (10–100 Å). The rate of formation of small-scale droplets proves to be two or three orders higher than that of the large droplets. In this work it is shown that the appearance of the above groups of microdroplets is due to two kinds of instability developed in an LMIS. The smaller droplets are due to the Rayleigh instability on the surface of thin cylindrical jets ejected from the tip of the Taylor cone at higher currents. This instability results in jet fragmentation and formation of small droplets (with sizes of the order of the jet radius) till the jet completely disappears. Following this the jet ejection reappears and the jet fragmentation process is repeated. Thus, the Rayleigh instability is accompanied by the comparatively low-frequency ion current oscillations ($f = 1$–10 MHz) which are due to the process of fragmentation and recovery of the jets. This process leads to the liquid-metal pressure modulation and causes the comparatively large-scale capillary wave extension on the Taylor cone surface as a result of the Faraday parametrical effect. It is this effect that leads to formation of the large droplets generated on the Taylor cone surface. We have made measurements of the angular distributions of the large and small droplets, as well as their intensities in the instability mode in tin LMIS. The measurements were carried out with transmission electron microscopy (TEM). The higher harmonic dependence of low frequencies on the current value have been defined. Also, the comparison between the computed and the experimental data have been carried out.

1. Introduction

The typical LMIS consists of sharpened high-melting metal needle. The liquid metal with high wetting ability goes up along the needle. If the voltage V is sufficiently high in space between the needle and the extractor, the liquid takes the Taylor cone shape [1]. At the cone apex [2], the fields are sufficiently large to induce ion evaporation directly from the liquid metal. The operation at higher currents induces a narrow liquid jet from the Taylor cone [2]. From the apex of this jet, the high-current emission is provided [3]. The above mentioned evolution of the emission geometry was first observed by Sudraud et al. [4,5] in Ga and Au sources. The electrostatic pressure on the jet apex dominates, pulling out a jet. However, the jet length h and radius a are fixed at given current values as a result of the process of intensive ion emission [3]. The electric field E on the tip of the jet is limited because of the space charge [2,3]: $E = E_i$, where E_i is the characteristic field for ion evaporation. Therefore, the current increase is only connected with the jet radius extension (emission site area) [3] which is also accompanied by elongation of the jet. A number of papers deal with the emission instability and the formation of liquid droplets at higher currents [4–7]. Below we show that the jet is unstable with respect to formation of sausage-like shapes (the Rayleigh instability [8]) which results in the formation of small droplets.

2. Calculation of the jet parameters

Let us determine the geometrical parameters of the cylindrical jet with a semispherical tip

0039-6028/92/$05.00 © 1992 – Elsevier Science Publishers B.V. All rights reserved

occurring on the cone, the base dimensions of which are much greater than those of the jet radius and length. In keeping with the conditions of the mass and momentum conservation it follows that [9]

$$a^2 = \frac{MI}{\pi e \rho U_0}, \quad v_0 = \frac{E_i}{\sqrt{8\pi\rho}} \sqrt{1 - \frac{16\pi\sigma}{aE_i^2}}, \qquad (1)$$

where I is current, ρ is the liquid density, M is the ion mass, e is the electron (ion) charge, v_0 is the velocity of jet and σ is the surface tension coefficient. The ratios (1) determine the jet radius and velocity dependence on a current value.

At higher currents ($a \gg 16\pi\sigma/E_i^2$)

$$a^2 = \frac{M}{eE_i} \sqrt{\frac{8}{\pi\rho}}\, I, \quad v_0 = E_i \sqrt{\frac{1}{8\pi\rho}}, \qquad (2)$$

i.e. the jet radius change is $\sim \sqrt{I}$, while the jet velocity remains constant. For tin ($E_i = 2.4 \times 10^{10}$ V/m, $\sigma = 0.4$ J/m^2) in accordance with eq. (1), at $I = 40$ μA $a = 20$ Å, $v_0 = 5.5 \times 10^2$ m/s; if $I = 120$ μA then $a = 35$ Å, $v_0 = 5.8 \times 10^2$ m/s.

The computed value of the jet length is determined by the expression [9]

$$h = R_0 \left(\frac{aE_i}{V} \right)^2, \qquad (3)$$

where R_0 is the distance from the vertex of needle to the extractor ($R_0 \gg h$). In case of the steep characteristics $I(V)$, $h \sim a^2 \sim I$. Making use of the experimental dependencies $I(V)$ and ratios (1) and (3), it is possible to determine the value of $h(I)$. The jet length and radius calculations [9] for corresponding current values using eqs. (1) and (3) have confirmed excellently the experimental data [5]. For the case of a tin LMIS from the measured dependence of $I(V)$ (see fig. 3, $R_0 = 5 \times 10^{-2}$ cm) it is possible to obtain: at $I = 40$ μA, $h = 190$ Å; at $I = 120$ μA, $h = 570$ Å.

We have computed [9] the lateral electric field distribution $\tilde{E}$ along the jet. When analyzing the stability, we used the average values of these fields (for Sn: $\tilde{E}_{av} = 0.35 E_i$ at $I = 40$ μA; $\tilde{E}_{av} = 0.3\ E_i$ at $I = 120$ μA).

3. The Rayleigh instability and the formation of small droplets

The Rayleigh instability [8] leading to jet fragmentation into droplets is due to the competition of the two kinds of surface tensions, the radial tension and the "wave" tension (resulting from the periodic modulated surface along the jet axis). When the lateral electric field is high enough there appears an additional mechanism of instability [10] shifting the maximum of the growth rate to the shorter wavelength region. The instability criterion is formed for the condition of the characteristic time t_0 of sausage development in the frame of reference that moves with the jet to be shorter than the time necessary for the liquid to flow along the jet length (h/v_0):

$$t_0 < h/v_0. \qquad (4)$$

According to eq. (4) the instability can occur only in sufficiently long jets. The value of t_0 can be estimated from maximum growth rate γ_m known from the linear theory [9,11]:

$$t_0 = (2\gamma_m)^{-1} \left[\ln \frac{\sigma}{K_B T K_m^2} + 2 \ln \left(1 + \frac{\nu K_m^2}{\gamma_m} \right) \right], \qquad (5)$$

where K_m is the wave number associated with the maximum growth rate, ν is the kinematic viscosity coefficient (for Sn $\nu \approx 10^{-7}$ m^2/s), $T \approx 2 \times 10^3$ K is the liquid temperature and K_B is the Boltzmann constant. Fig. 1 shows the data of the numerical calculations of the sausage dispersion ratio [9] for liquid tin with due regard for the lateral electric field and the viscosity for the currents of 40 and 120 μA. Thus it is evident that criterion (4) for these currents is justified. The instability threshhold corresponds to a current of 30 μA. It should be pointed out here that for $\tilde{E} = 0$ (case the which was considered by Rayleigh [8]) the growth rate $\gamma > 0$ only if $X = Ka < 1$ (fig. 1). The shift of growth rate maximum towards the $Ka > 1$ region is connected with the effect of the lateral electric field.

The radius R of initial droplets, detaching from the jet as a result of sausage development, can be evaluated by means of the relation $\pi a^2 \lambda_m$

$= \frac{4}{3}\pi R^3$, where $\lambda_m = 2\pi/K_m$. It gives: $R = a(3\pi/2X_m)^{1/3}$. For $I = 40$ μA, $R = 1.4a \approx 28$ Å, while in case of $I = 120$ μA, $R = 1.3a \approx 45$ Å. The initial droplet carries a large charge and they must break up into smaller fragments ($R = 15$–20 Å) according to the Rayleigh instability criterion [12]. The sausage development can be accompanied by the formation of satellite droplets [13] which have a radius three times smaller than that of the large ones ($R \approx 10$–15 Å) [14]. Thus, the initial stage of jet decay has already been accompanied by microdroplet chaos (the droplets emitted are characterized by a wide spread of their dimensions). The microdroplet chaos is enchanced further. This is connected with the lateral electric field of remaining part of the jet, which is decreased due to potential screening by the charged droplets. Correspondingly, the decrease of the lateral electric field results in sausage wavelength growth (fig. 1) and the radius of the droplets increase. When the capillary and electrostatic pressures become equal on the jet tip the latter breaks up completely. A probable picture of micro-droplet chaos is presented in fig. 2.

After the jet decays and the droplet leaves the near region of the jet, the jet is re-established and the process of the jet decay recurs. An increase in current results in an increase in jet decay time because in this case the jet is longer, and the

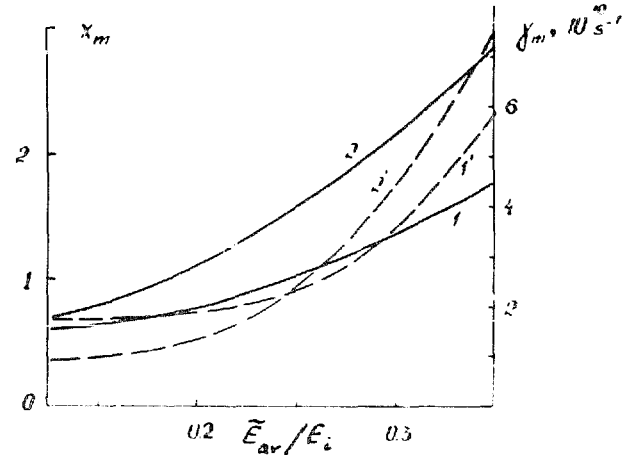

Fig. 1. Wavelength $X_m = 2\pi a/\lambda_m$ corresponding to the growth rate in its maximum γ_m (solid line) and γ_m as a function of lateral electric field (dashed line). Curves 1, 1′ at $I = 40$ μA; Curves 2, 2′ at $I = 120$ μA.

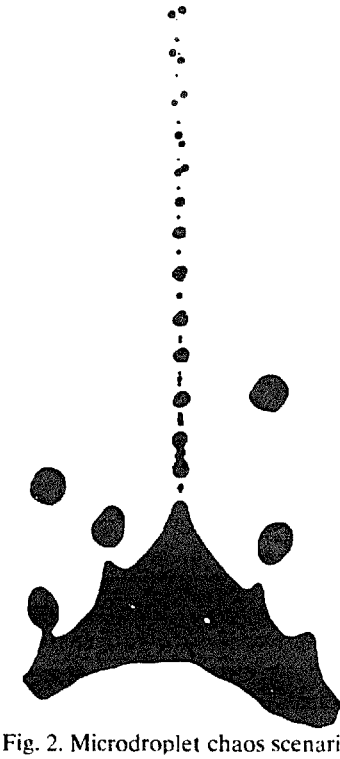

Fig. 2. Microdroplet chaos scenario.

electrostatic and capillary pressure equilibrium occurs in a smaller electric field (the jet radius being large). Numerical methods have shown a decay time of $\tau_d = 5 \times 10^{-8}$ s at $I = 40$ μA, and 2.7×10^{-7} s at $I = 120$ μA. Under the condition that τ_1 corresponds to the current oscillation cycle, $f = 1/\tau_d = 20$ MHz, and $f = 4$ MHz at $I = 120$ μA. Thus, as the current increases, the frequency of oscillations is decreased noticeably. During the course of the decay at $I = 40$ μA, the droplet number is $N = 5 \times 10^2$, and at $I = 120$ μA, $N = 2 \times 10^3$. The intensity of droplets formation (N/τ_d) depends to some extent on the current beyond the Rayleigh instability threshold ($N/\tau_d \approx 10^{10}$ s^{-1}).

4. The Faraday instability and large droplet formation

The periodic process of jet decay and re-establishment causes a pressure modulation in the liquid at a frequency $f = 1/\tau_d$ that leads to capillary waves parametrical excitation (the Fara-

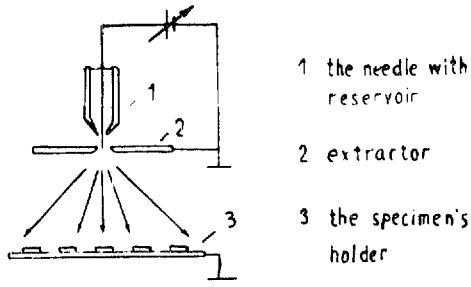

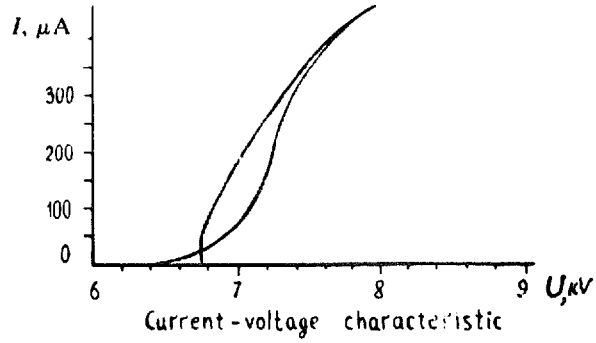

Fig. 3. Experimental scheme and Sn LMIS $I(V)$ curves.

day effect [15]) on the Taylor's cone surface accompanied by large droplets tearing off the peaks of the capillary waves. Under the condition of resonance:

$$\omega_c = 2\pi f, \; f = 1/\tau_d, \tag{6}$$

where $\omega_c = \sqrt{\sigma K_c^3/\rho}$ is the frequency of capillary wave [8], K_c is the wave number. It follows that

$$\lambda_c = \frac{2\pi}{K_c} = \left(\frac{2\pi\sigma\tau_d^2}{\rho}\right)^{1/3}. \tag{7}$$

At $I = 40$ μA, $\lambda_c \approx 10^4$ Å; at $I = 120$ μA, $\lambda_c = 3 \times 10^4$ Å. Correspondingly, the large droplet radius ($R \approx 1/K_c$) is 10^3 Å and 3×10^3 Å. The intensity of such droplets formation is equal to $\approx 10^7$ s^{-1} provided that several droplets are coming off during the oscillation cycle. Thus, the intensity of large droplets formation is two to three orders of magnitude smaller than that of the small ones. Earlier this fact was pointed out by Thompson [16].

5. Experiments

Our experiments were conducted using a Sn LMIS with a steel needle, the surface of which was mechanically processed in order to create a developed system of grooves on it. It enabled the needle to possess low hydrodynamical impedance. The radius of curvature of needle's apex was about 10 μm. The hole of 0.2 cm in diameter served to let the droplet fraction come through the extractor, depositing on a system of TEM specimens located at the distance of 5 cm from the extractor. The diameter of a TEM specimen is equal to 0.3 cm. The distance between the specimens in $d = 1$ cm. The scheme of the experiment as well as $I(V)$ curves of ion sources studied are presented in fig. 3. The reservoir containing Sn was located at the base of the needle and supplied with intensive heating. For the unstable

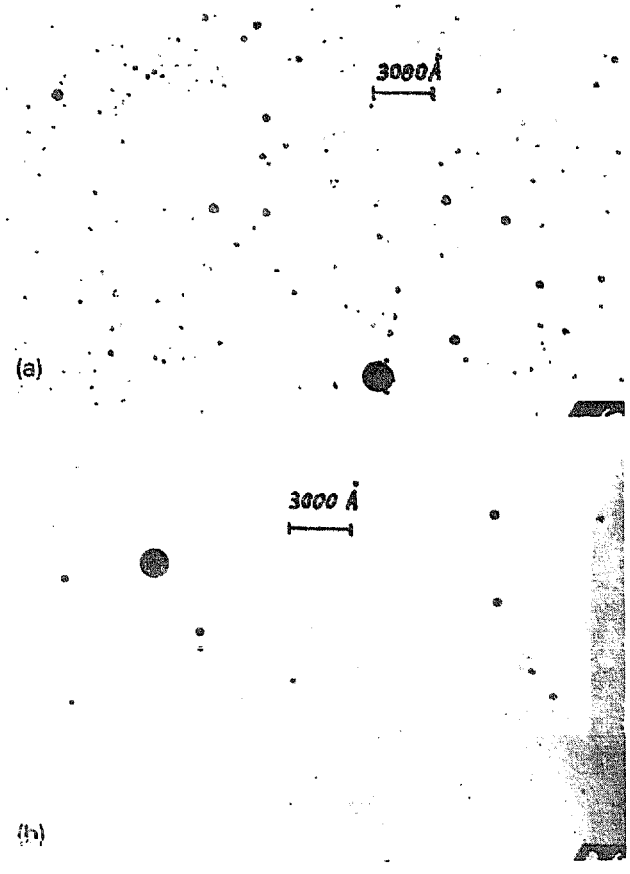

Fig. 4. The pictures of separate areas of (a) the central and (b) the periferical ($d = 1$ cm) specimens at $I = 120$ μA.

mode of LMIS the time of specimens exposure was equal to 10 s. The droplet size distribution was studied by means of TEM. The data are given in fig. 4 which shows the smaller droplet deposition mainly in the central specimens. The quantity of the larger droplets is small, which can be seen on those specimens. Fig. 5 presents the droplet distribution according to their size in the central specimen. Later on, considering that the smaller droplets ($R < 100$ Å) are deposited on the area as large as the area of a separate specimen, the rate of the small droplet formation is $\approx 10^{10}$ s^{-1}. The rate of large droplet formation is three orders smaller. Thus, the small droplet distribution is comparatively dense whereas that of the large ones is rather discrete. The distribution of this kind as well as its deposition mode is in qualitative accordance with the microdroplet chaos scenario of small droplet formation and the

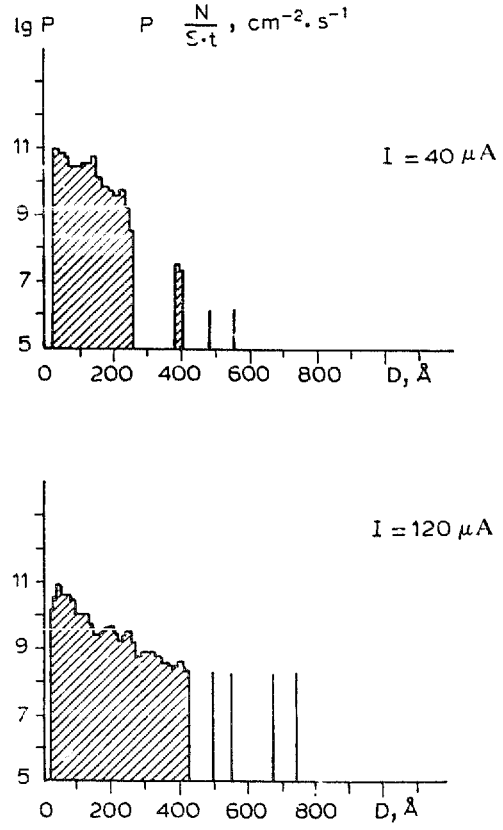

Fig. 5. Dependence of microdroplet formation intensity on their size for different currents, shown in the central specimen.

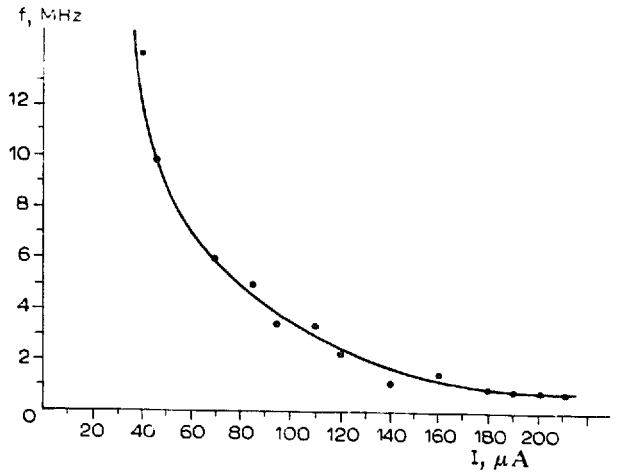

Fig. 6. Dependence of the higher harmonic of the ion current oscillations on current values.

resonance mechanism of the large dorplet formation.

Fig. 6 shows the current oscillation dependence on the current value. The results shown above are in qualitative and quantitative accordance with our calculations.

6. Summary

This study shows that the basic principles of the droplet emission mechanism in LMIS are based on the classical ideas by Faraday [15], Rayleigh [8,12], Taylor [1], Gomer [2], and Kingham and Swanson [3]. The LMIS turns into an intensive microdroplet emitter ($R \approx 10$–200 Å) with sufficiently high currents. These results may have a practical interest for deposition of different kinds of coatings.

References

[1] G.I. Taylor, Proc. R. Soc. London A 280 (1964) 383.
[2] R. Gomer, Appl. Phys. 19 (1979) 365.
[3] D.R. Kingham and L.W. Swanson, Appl. Phys. A 34 (1984) 123.
[4] H. Gaubi, P. Sudraud, M. Tence and J. van de Walle, in: Proc. 29th Int. Field Emission Symp. Göteborg (1982) p. 357.
[5] G. Benassayag, P. Sudraud and B. Jouffrey, Ultramicroscopy 16 (1985) 1.

[6] G.L.R. Mair and J. von Engel, J. Appl. Phys. 50 (1979) 5592.
[7] D.L. Barr and W.L. Brown, J. Vac. Science & Technol. (1989) 1806.
[8] Lord Rayleigh, Proc. London Math. Soc. 10 (1878) 4.
[9] V.V. Vladimirov and V.N. Gorshkov, JTP (USSR) 57 (1987) 2155.
[10] L. Tonks, Phys. Rev. 48 (1935) 562;
Ya.I. Frenkel, Phys. Z. Sowiet-Union 8 (1935) 675.
[11] S.S. Nazin, A.N. Izotov and V.B. Shikin, DAN USSR 283 (1985). 121.
[12] Lord Rayleigh, Proc. R. Soc. London 29 (1879) 71.
[13] R.S. Donnely and W. Glaberson, Proc. R. Soc. London A 290 (1966) 574.
[14] V.V. Vladimirov and V.N. Gorshkov, JTP (USSR) 60, 11 (1990)) 197.
[15] M. Faraday, Philos. Trans. R. Soc. London (1831) 299.
[16] S.P. Thompson, Proc. 29th Int. Field Emission Symp., Göteborg (1982) p. 349.

The author has requested enhancement of the downloaded file. All in-text references underlined in blue are linked to publications on ResearchGate